Hydrogen Production

International Edition: DOI: 10.1002/anie.201506797
German Edition: DOI: 10.1002/ange.201506797

Stable Co-Catalyst-Free Photocatalytic H_2 Evolution From Oxidized Titanium Nitride Nanopowders

*Xuemei Zhou, Eva M. Zolnhofer, Nhat Truong Nguyen, Ning Liu, Karsten Meyer, and Patrik Schmuki**

Abstract: *A simple strategy is used to thermally oxidize TiN nanopowder (~20 nm) to an anatase phase of a TiO_2:Ti^{3+}:N compound. In contrast to the rutile phase of such a compound, this photocatalyst provides activity for hydrogen evolution under AM1.5 conditions, without the use of any noble metal co-catalyst. Moreover the photocatalyst is active and stable over extended periods of time (tested for 4 months). Importantly, to achieve successful conversion to the active anatase polymorph, sufficiently small starting particles of TiN are needed. The key factor for catalysis is the stabilization of the co-catalytically active Ti^{3+} species against oxidation by nitrogen present in the starting material.*

In 1972, Fujishima and Honda reported groundbreaking work on the photolytic cleavage of water to H_2 and O_2.[1] Since then, the concept of using solar light and a suitable semiconductor to generate H_2 has received tremendous scientific attention. In their experiments, Fujishima and Honda used a two-electrode approach with a TiO_2 single crystal as an illuminated photoanode and a Pt sheet as a counter electrode for hydrogen evolution (a photoelectrochemical configuration).

A more straightforward approach is to use a suspension of nanoparticles (that is, without external electrochemical bias), where the photogenerated holes and electrons from the same particle react with the surrounding water. However, under these conditions, the presence of a suitable co-catalyst on the TiO_2 particles is required in order to efficiently generate H_2. Over the past decades, in virtually any investigation on photocatalytic hydrogen evolution, noble metals, such as Pt, Au, Pd,[2] have been used as they are the most effective co-catalysts owing to their ability to act as electron transfer mediator and recombination center for H_2. Efforts to replace these expensive noble metal co-catalysts are limited to only a few reports.[2a,3]

A key factor to form noble-metal-free active material may be the formation of a specific configuration of Ti^{3+}/O_v (O_v = oxygen vacancies) on anatase particles. However, well established reduction treatments of TiO_2 known to form Ti^{3+}/O_v species (such as heat treatment in vacuum, Ar, Ar/H_2, ion bombardment, or cathodic reduction)[2a,4] lead to a non-stable co-catalytic effect owing to how readily oxidized Ti^{3+} is in air or aqueous environments.[3a,b,5]

An alternative approach to form Ti^{3+}-rich TiO_2 is, in principle, to perform a controlled partial oxidation of Ti^{III} compounds instead of a partial reduction of TiO_2. From previous work,[5,6] we know that the two key requirements to obtain a stable and active catalyst are: i) the stabilization of the remaining Ti^{III} against further oxidation, and ii) the formation of an anatase type of polymorph TiO_2 by oxidation (rutile is reported not to be active). To address requirement (i), theoretical work combined with experimental evidence indicate that nitrogen species situated in interstitial and/or substitutional positions are capable of stabilizing Ti^{3+} centers by charge transfer resonance, as suggested by Livraghi, Hoang, and co-workers.[7] Therefore the question arises, if an optimized oxidation of TiN may lead to a nitrogen stabilized Ti^{3+} configuration and could also result, when oxidized, in an anatase form of TiO_2 (and thereby also address ii).

Some previous attempts to thermally oxidize TiN were mainly undertaken to create N-doped TiO_2 with the intent to alter the light absorption properties towards a visible light response to provide an alternative to other nitrogen doping methods (such as ammonolysis,[8] ion implantation[9] and co-precipitation),[10] with the aim to create band-gap narrowing in TiO_2 (ascribed to a mixing of N 2p-states with the O 2p valence band states of TiO_2).[11,12a] Previous work on the oxidation of TiN used either comparably large particles or surface films that in any reported case evolved, upon thermal oxidative treatment, to a rutile phase.[12] This polymorph is undesired for our purposes, since in previous work a H_2 evolving co-catalytic Ti^{3+}-state was only obtained for anatase.[6a,3c] Rutile is the thermodynamically stable form of titania under a broad range of conditions. However, various theoretical work reports that at the nanoscale (typically < 30 nm), anatase can become the thermodynamically stable polymorph.[3a,13]

Herein, we explore the use of TiN nanoparticles (ca. 20 nm) for a controlled partial thermal oxidation and investigate the photocatalytic properties, composition, and structure at various stages of oxidation. We show that such TiN nanoparticles can be oxidized to an anatase-type titania photocatalyst that carries stable, intrinsic co-catalytic centers for hydrogen evolution, facilitating stable photocatalytic H_2 production at enhanced rates without the use of noble metal

[*] X. Zhou, N. T. Nguyen, Dr. N. Liu, Prof.Dr. P. Schmuki
Department of Materials Science WW-4, LKO
University of Erlangen-Nuremberg
Martensstrasse 7, 91058 Erlangen (Germany)
E-mail: schmuki@ww.uni-erlangen.de
E. M. Zolnhofer, Prof.Dr. K. Meyer
Friedrich-Alexander University Erlangen-Nürnberg (FAU)
Department of Chemistry and Pharmacy, Inorganic Chemistry
Egerlandstrasse 1, 91058 Erlangen (Germany)

Supporting information for this article is available on the WWW under http://dx.doi.org/10.1002/anie.201506797.

co-catalysts (Figure 1). Figure 1 a shows the measured initial photocatalytic hydrogen evolution rates under AM1.5 (100 mW cm^{-2}) conditions for various oxidized TiN powder samples as well as for various reference samples (namely anatase and reduced anatase). Experimental details are given in the Supporting Information (Figure S1). To produce oxidized TiN, commercial TiN (20 mg) of an average grain size of approximately 20 nm was annealed in air under different conditions (300 °C–450 °C for 30 min–9 h). A suspension of this sample was prepared and the photocatalytic activity for H_2 evolution was measured over time. Partially reduced anatase samples (fabricated by thermal Argon or Argon/H_2 treatment)[3b,5e–f,14] were used as reference samples to provide a comparison to conventionally reduced Ti^{3+}-containing material without any nitrogen-stabilizing effects. As shown in Figure 1 a, various annealing treatments of TiN in air lead to a product that yields a significantly enhanced photocatalytic activity for H_2 evolution compared to pure anatase (without using any noble metal co-catalyst). While for pure titanium nitride, or samples that were annealed up to 300 °C, no photocatalytic hydrogen could be detected. Treatments with temperatures higher than 350 °C clearly showed photocatalytic activity for H_2 evolution. By investigating a range of annealing conditions, varying temperature and time (Supporting Information, Figure S1), we have found that the optimal conditions for air annealing are either at 400 °C for 1 h, or similarly at 350 °C for 5 h. An estimation of the quantum efficiency of the process under our best conditions is given in the Supporting Information.

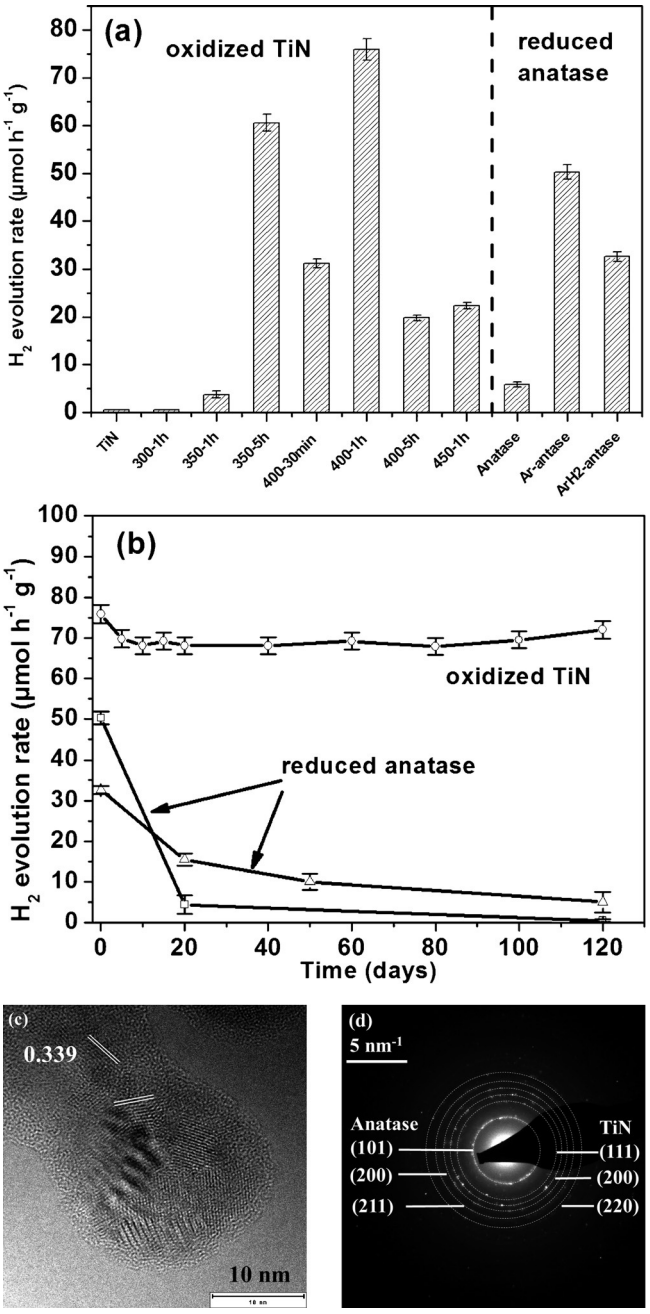

Figure 1. (a) Open-circuit hydrogen generation for oxidized TiN nanopowders treated at different temperatures in air and comparison to reduced anatase samples as a reference. (b) Stability of photocatalytic H_2 evolution for oxidized TiN (400 °C, 1 h) and reduced anatase (△: Ar/H_2 500 °C, 3 h; □: Ar 500 °C, 3 h). H_2 evolution experiments were performed under AM1.5 (100 mW cm^{-2}) at room temperature in 50% methanol/H_2O electrolyte without the presence of any co-catalyst. (c) TEM and (d) corresponding SAED patterns for oxidized TiN (TiN 350 °C–3 h, that is, optimized photocatalyst).

Most importantly, Figure 1 b shows that the intrinsic catalytic activity of this oxidized TiN material is stable over time and in repeated experiments. In contrast, reduced anatase samples (Ar, Ar/H_2) show some initial activity (Figure 1 b) that, however, is quickly lost after 2 or 3 photocatalysis experiments. In fact, for TiN the data show that the H_2 evolution rate remains constant over a period of over 4 months (longest measured duration). These findings suggest that the combination of nitrogen and Ti^{3+} states leads to a remarkably stable catalytic center for H_2 evolution without the use of a co-catalyst. It is noteworthy that measurements taken with a 420 nm cut-off filter did not show any significant H_2 evolution, that is, the main effect of nitrogen is the stabilization of the UV photocatalytic activity.

Figure 1 c shows the HRTEM image and the corresponding SAED pattern (Figure 1 d) from an activated grain of the photocatalyst. The SAED pattern confirms the presence of a mixture of anatase and TiN after annealing. In the HRTEM in Figure 1 c, lattice fringes of $d = 0.34$ nm were determined, corresponding to a typical lattice spacing of anatase (101). Moreover, the thermal treatment does not change the morphology nor the size of the particle significantly (Supporting Information, Figure S2). It may also be noted that the conversion of TiN to the active catalyst material can easily be followed by eye, as the initially black color of the TiN is changed to grey by annealing (Supporting Information, Figure S2 g).

To follow the structural and compositional changes during the annealing treatments, the different oxidation stages were characterized by XRD (Figure 2; Supporting Information, Figure S3), Raman spectroscopy (Supporting Information, Figure S4), and XPS (Figure 3; Supporting Information, Figure S5).

Figure 2 shows the XRD patterns of the nanoscale TiN samples (SEM; Supporting Information, Figure S2 a) annealed in air in the temperature range from 300 °C to

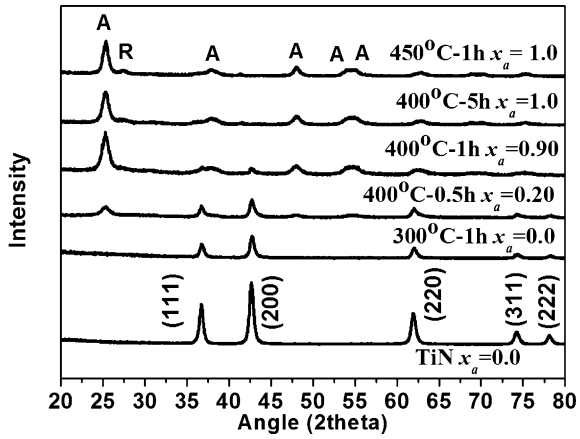

Figure 2. XRD patterns for untreated titanium nitride and after annealing at 300 °C, 400 °C, 450 °C. *Xa* is the fraction of anatase in the mixture by calculation from the integrated intensities of the (101) reflection of anatase and the (200) reflection of titanium nitride.

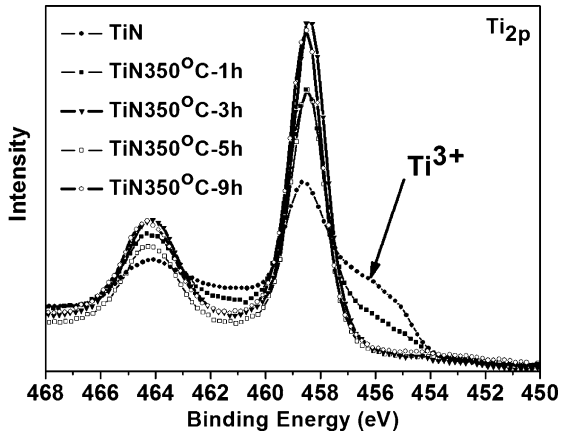

Figure 3. High resolution XPS Ti2p peaks for TiN nanopowders and oxidized TiN at 350 °C for 1 h to 9 h, respectively.

450 °C for 1 h. The XRD pattern of the originally 20 nm titanium nitride materials can be assigned to osbornite, cubic phase (PDF card No. 00-038-1420), presenting a main peak at 42.6°. With increasing temperature, the intensity of the XRD peak for TiN decreases while the peak intensity of the TiO_2 anatase phase (PDF card No. 00-021-1272, Tetragonal) increases. For annealing at 400 °C for 1 h, clear anatase peaks become apparent; and at a temperature of 450 °C, also traces of rutile (PDF card No. 00-021-1276, Tetragonal) become visible, while no TiN peaks can be detected anymore. The formation of anatase in the TiN particles can also be observed by Raman spectroscopy (Supporting Information, Figure S4), with characteristic absorption bands at 145, 396.0, 514.6, and 637.7 cm^{-1} (Supporting Information, Figure S4a). For the nanoscale-catalyst-material, peak shifts and broadening is observed (TiN 400 °C–1 h; Supporting Information, Figure S4b) compared to pure anatase reference powder. This may be related to confined lattice vibrations and structural defects[15] for the nitrogen-doped TiO_2 nanomaterial. To study annealing-time related effects of the conversion, we kept a TiN (20 nm) sample at 350 °C for various times (Supporting Information, Figure S3b). With increasing annealing time, the anatase content (X_a) can be increased from 0.043 to 0.96. This is also observed at an annealing temperature of 400 °C, when annealing times from 30 min to 5 h are used, the content of anatase increases from 0.20 to 1.0.

Figure 3 provides high resolution XPS spectra of selected samples before thermal treatment and at different oxidation states, clear alterations of Ti2p peaks, as well as of N1s peaks are observed after annealing in air. The Ti2p peak for TiN appears with a strong typical Ti^{3+} tail below 457 eV (Figure 3). During annealing at 350 °C, the intensity of this tail decreases, and for annealing for longer than 3 h the Ti^{3+} is almost fully oxidized to Ti^{4+} (within the penetration depth of XPS). Correspondingly, significant changes of the N1s peak can be observed before and after annealing (Supporting Information, Figure S5). The high resolution N1s peak for TiN, located at binding energies of 396.9 eV and 395.8 eV, is commonly ascribed to a nitride compound and to substitutional nitrogen in TiO_2. After annealing at 350 °C, the intensity of peaks between 396–397 eV decreases and new peaks at a binding energy of 402 eV appear. These peaks can be assigned to surface bound NO_x-species that probably are released from the lattice during oxidation.[16] After annealing at 350 °C for 5 h or higher temperatures, the only traceable N peak is this 402 eV signature. However, in XRD, for the TiN samples annealed at 400 °C for 1 h and TiN 350 °C for 5 h, the crystalline TiN diffraction peak at 42.6° is still visible after the thermal treatment. This indicates that the majority of TiN remains as a core of the particle while at the stronger oxidized surface, nitrogen is only left at very low concentrations (below the detection limit of XPS). During the thermal annealing, a change in the high resolution O1s peak can also be seen (Supporting Information, Figure S5a). Generally, the intensity of the O1s peak located at a binding energy of 529.8 eV (oxide) increases, which can be ascribed to the formation of TiO_2, while the peak intensity at a higher binding energy (usually assigned to surface OH) decreases. Overall, the XPS data are well in line with the formation of TiO_2 surrounding a TiN core. A quantitative evaluation of peak intensities is compiled in the Supporting Information (Table S1). It is clear that with an increase in annealing time and temperature, the ratio of N/O in the TiN samples decreases from 0.456 to 0.0133, in agreement with a transition from TiN to TiO_2.

Additionally, we characterized the samples with electron paramagnetic resonance spectroscopy (EPR) that is widely used in the characterization of paramagnetic centers, such as Ti^{3+} or oxygen vacancy species present in TiO_2.[17] Figure 4a shows the EPR spectra for the active TiN-based catalyst generated by an air-heat treatment (400 °C–1 h) and a reference sample, where Ti^{3+}-species were generated by an Ar-heat treatment (500 °C–3 h). The EPR spectra were measured directly after the thermal treatment and after aging the samples for four months (air exposure and regular H_2 photoactivity measurements). The EPR spectra of all four samples exhibit a signal at a *g*-value of $g = 1.997$, which is attributed to a Ti^{3+} defect in the sample.[17e,18] In both fresh samples (TiN400-1h fresh and Ar-anatase fresh) as well as the aged sample (TiN400-1h after 4 months), additional low-intensity

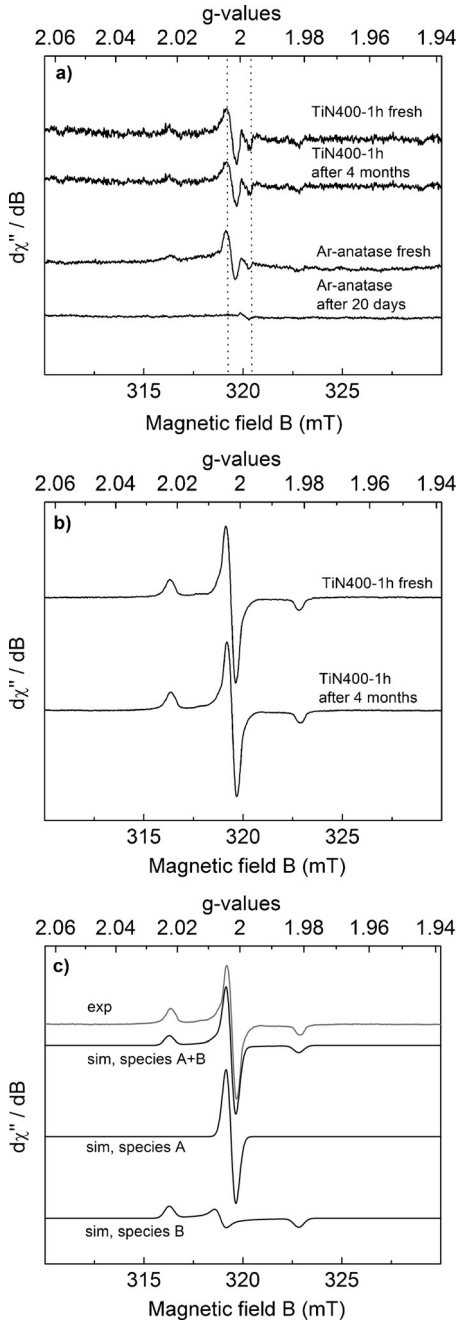

Figure 4. CW X-band EPR spectra of oxidized titanium nitride (400 °C, 1 h) directly after preparation and after aging for 4 months, recorded in the solid state at RT and 100 K. Experimental conditions: microwave frequency = 8.96 GHz, modulation width = 0.5 mT, microwave power = 1 mW, modulation frequency = 100 kHz, time constant = 0.1 s. (a) Comparison of oxidized titanium nitride to Ar-reduced anatase (freshly prepared and aged) measured at *RT*. (b) EPR spectra of TiN 400 °C–1 h, freshly prepared and after aging for 4 months, measured at 100 K under illumination. (c) EPR spectrum of TiN400 °C taken at 100 K under illumination (grey line) and its simulation (two species, black lines). Simulation parameters: Species A: weight = 1.00, $S = 1/2$, $g1 = 2.0031$, $g2 = 2.0026$, $g3 = 2.0012$, $W1 = 0.31$ mT, $W2 = 0.25$ mT, $W3 = 0.28$ mT. Species B: weight = 2.75, $S = 1/2$, $g1 = 2.0220$, $g2 = 2.0056$, $g3 = 1.9810$, $W1 = 0.28$ mT, $W2 = 0.27$ mT, $W3 = 0.30$ mT.

signals are shown in the range of $g = 1.97$–2.03 (obtained at RT under dark conditions). Upon illumination at 100 K, the intensity of the additional signals is highly increased owing to the photochemical generation of additional paramagnetic centers (Figure 4b). The better signal-to-noise ratio facilitates the simulation of the EPR signals, which reveals the presence of two species (Figure 4c): one highly isotropic signal with g-values of $g1 = 2.0031$, $g2 = 2.0026$, and $g3 = 2.0012$ (species A, assignable to F-centers or oxygen vacancies)[17] and one rhombic signal with g-values of $g1 = 2.0220$, $g2 = 2.0056$, and $g3 = 1.9810$ (species B, assignable to a Ti^{3+}/N_b-characteristic feature;[7,19] see also the Supporting Information). Most importantly, after aging, a clear difference in the spectra between the TiN 400 °C–1 h sample and the Ar-anatase sample is evident: while the signals for the nitride sample remains stable upon aging for four months, the reference sample shows a strong decrease of the signal intensity over 20 days. This indicates that re-oxidation of the locally reduced anatase sample eliminates the Ti^{3+}/O_v centers to a large extent (below the resolution limit of EPR). The high stability of the TiN 400 °C–1 h sample is also evident when investigated at 100 K under illumination in an air atmosphere (Figure 4) and other conditions (Supporting Information, Figure S6): in all measurements, the fresh TiN 400 °C–1 h (Figure 4b) as well as the four-months-aged sample (Figure 4c) give virtually identical signals of comparable intensity and hence are in line with the long-term stability of the catalytically active species (for example, the hydrogen evolution activity in Figure 1b). The EPR measurements also strongly support the concept of charge-transfer resonance being the origin of the N-stabilization effect of Ti^{3+} in thermally oxidized TiN nanoparticles; an explanation in terms of an electron transfer equilibrium between $Ti^{3+}/N_b \leftrightarrow Ti^{4+}/N_b^-$ as suggested by Selloni and coworkers[7b] seems plausible.

In summary, the present work shows that TiN nanoparticles (if sufficiently small) not only can be successfully converted to an anatase based TiO_2 photocatalyst, but more importantly, the material shows a highly stable photocatalytic H_2-production performance (tested over 4 months) without the use of any noble metal co-catalyst. EPR spectra further confirm the remarkably stable photocatalytic activity observed for these samples over time and further support the concept of a Ti^{3+} related defect structure capable of acting as a co-catalytic center for H_2 evolution.

Sample preparation and additional characterization results are shown in the Supporting Information.

Acknowledgements

The authors would like to thank Manuel Schweiger and Prof. Dr. Jana Zaumseil for the Raman measurements. We would also like to thank ERC, DFG and the EAM cluster of excellence for financial support.

Keywords: anatase · H_2 evolution · nanopowders · nitrogen stabilization · titanium

How to cite: *Angew. Chem. Int. Ed.* **2015**, *54*, 13385 – 13389
Angew. Chem. **2015**, *127*, 13583 – 13587

[1] A. Fujishima, K. Honda, *Nature* **1972**, *238*, 37 – 38.
[2] a) X. Chen, S. Shen, L. Guo, S. Mao, *Chem. Rev.* **2010**, *110*, 6503 – 6570; b) K. Connelly, A. K. Wahab, H. Idriss, *Mater. Renew. Sustain. Energy* **2012**, *1*, 3; c) M. Ni, M. K. H. Leung, D. Y. C. Leung, K. Sumathy, *Renewable Sustainable Energy Rev.* **2007**, *11*, 401 – 425; d) K. Lee, R. Hahn, M. Altomare, E. Selli, P. Schmuki, *Adv. Mater.* **2013**, *25*, 6133 – 6137; e) X. Chen, L. Liu, P. Y. Yu, S. S. Mao, *Science* **2011**, *331*, 746 – 750; f) B. Ohtani, Y. Ogawa, S. Nishimoto, *J. Phys. Chem. B* **1997**, *101*, 3746 – 3752; g) J. B. Priebe, J. Radnik, A. J. J. Lennox, M. Pohl, M. Karnahl, D. Hollmann, K. Grabow, U. Bentrup, H. Junge, M. Beller, A. Brückner, *ACS Catal.* **2015**, *5*, 2137 – 2148; h) G. Wang, H. Wang, Y. Ling, Y. Tang, X. Yang, R. C. Fitzmorris, C. Wang, J. Z. Zhang, Y. Li, *Nano Lett.* **2011**, *11*, 3026 – 3033.
[3] a) K. Lee, A. Mazare, P. Schmuki, *Chem. Rev.* **2014**, *114*, 9385 – 9454; b) I. Paramasivam, H. Jha, N. Liu, P. Schmuki, *Small* **2012**, *8*, 3073 – 3103; c) A. Fujishima, X. Zhang, D. A. Tryk, *Surf. Sci. Rep.* **2008**, *63*, 515 – 582; d) J. R. McKone, B. Sadtler, C. A. Werlang, N. S. Lewis, H. B. Gray, *ACS Catal.* **2013**, *3*, 166 – 169; e) P. G. M. B. Hinnemann, J. Bonde, K. P. Jørgensen, J. Nielsen, *J. Am. Chem. Soc.* **2005**, *127*, 5308 – 5309.
[4] a) U. Diebold, *Surf. Sci. Rep.* **2003**, *48*, 53 – 229; b) M. Anpo, M. Takeuchi, *J. Catal.* **2003**, *216*, 505 – 516; c) F. Zuo, L. Wang, T. Wu, Z. Zhang, D. Borchardt, P. Feng, *J. Am. Chem. Soc.* **2010**, *132*, 11856 – 11857; d) T. L. Thompson, J. Yates, *Chem. Rev.* **2006**, *106*, 4428 – 4453.
[5] a) X. Zhou, N. Liu, P. Schmuki, *Electrochem. Commun.* **2014**, *49*, 60 – 64; b) A. Naldoni, M. Allieta, S. Santangelo, M. Marelli, F. Fabbri, S. Cappelli, C. Bianchi, R. Psaro, V. D. Santo, *J. Am. Chem. Soc.* **2012**, *134*, 7600 – 7603; c) A. Teleki, S. E. Pratsinis, *Phys. Chem. Chem. Phys.* **2009**, *11*, 3742 – 3747; d) K. Komaguchi, T. Maruoka, H. Nakano, I. Imae, Y. Ooyama, Y. Harima, *J. Phys. Chem. C* **2010**, *114*, 1240 – 1245; e) J. M. Macak, H. Tsuchiya, A. Ghicov, K. Yasuda, R. Hahn, S. Bauer, P. Schmuki, *Curr. Opin. Solid State Mater. Sci.* **2007**, *11*, 3 – 18; f) C. N. Rusu, J. J. T. Yates, *Langmuir* **1997**, *13*, 4311 – 4316.
[6] a) N. Liu, C. Schneider, D. Freitag, U. Venkatesan, V. R. R. Marthala, M. Hartmann, B. Winter, E. Spiecker, A. Osvet, E. M. Zolnhofer, K. Meyer, T. Nakajima, X. Zhou, P. Schmuki, *Angew. Chem. Int. Ed.* **2014**, *53*, 14201 – 14205; *Angew. Chem.* **2014**, *126*, 14425 – 14429; b) N. Liu, C. Schneider, D. Freitag, M. Hartmann, U. Venkatesan, J. Müller, E. Spiecker, P. Schmuki, *Nano Lett.* **2014**, *14*, 3309 – 3313.
[7] a) S. Hoang, S. Berglund, N. Hahn, A. Bard, C. Mullins, *J. Am. Chem. Soc.* **2012**, *134*, 3659 – 3662; b) S. Livraghi, M. C. Paganini, E. Giamello, A. Selloni, C. D. Valentin, G. Pacchioni, *J. Am. Chem. Soc.* **2006**, *128*, 15666 – 15671; c) C. Di Valentin, E. Finazzi, G. Pacchioni, A. Selloni, S. Livraghi, M. Paganini, E. Giamello, *Chem. Phys.* **2007**, *339*, 44 – 56; d) M. Batzill, E. H. Morales, U. Diebold, *Chem. Phys.* **2007**, *339*, 36 – 43.
[8] R. P. Vitiello, J. M. Macak, A. Ghicov, H. Tsuchiya, L. F. P. Dick, P. Schmuki, *Electrochem. Commun.* **2006**, *8*, 544 – 548.
[9] a) A. Ghicov, J. M. Macak, H. Tsuchiya, J. Kunze, V. Haeublein, L. Frey, P. Schmuki, *Nano Lett.* **2006**, *6*, 1080 – 1082; b) A. Ghicov, J. M. Macak, H. Tsuchiya, J. Kunze, V. Haeublein, S. Kleber, P. Schmuki, *Chem. Phys. Lett.* **2006**, *419*, 426 – 429.
[10] a) J. L. Gole, J. D. Stout, C. Burda, Y. Lou, X. Chen, *J. Phys. Chem. B* **2004**, *108*, 1230 – 1240; b) X. Chen, Y.-B. Lou, A. Samia, C. Burda, J. Gole, *Adv. Funct. Mater.* **2005**, *15*, 41 – 49.
[11] a) G. Liu, H. G. Yang, X. Wang, L. Cheng, J. Pan, G. Q. (Max) Lu, H. M. Cheng, *J. Am. Chem. Soc.* **2009**, *131*, 12868 – 12869; b) X. Li, J. Yu, J. Low, Y. Fang, J. Xiao, X. Chen, *J. Mater. Chem. A* **2015**, *3*, 2485 – 2534; c) Q. Xiang, J. Yu, W. Wang, M. Jaroniec, *Chem. Commun.* **2011**, *47*, 6906 – 6908; d) J. Buha, *Appl. Surf. Sci.* **2014**, *321*, 457 – 463; e) N. Wu, Y. Wang, Y. Lei, B. Wang, C. Han, *Appl. Surf. Sci.* **2014**, *319*, 136 – 142; f) A. Petala, D. Tsikritzis, M. Kollia, S. Ladas, S. Kennou, D. I. Kondarides, *Appl. Surf. Sci.* **2014**, *305*, 281 – 291; g) P. Zhou, J. Yu, Y. Wang, *Appl. Catal. B* **2013**, *142 – 143*, 45 – 53.
[12] a) R. Asahi, T. Morikawa, H. Irie, T. Ohwaki, *Chem. Rev.* **2014**, *114*, 9824 – 9852; b) L. Wan, J. Li, J. Feng, W. Sun, Z. Mao, *Appl. Surf. Sci.* **2007**, *253*, 4764 – 4767; c) S.-M. Oh, J.-G. Li, T. Ishigakia, *J. Mater. Res.* **2005**, *20*, 529 – 537.
[13] a) M. R. Ranade, A. Navrotsky, H. Z. Zhang, J. F. Banfield, S. H. Elder, A. Zaban, P. H. Borse, S. K. Kulkarni, G. S. Doran, H. J. Whitfield, *Proc. Natl. Acad. Sci. USA* **2002**, *99*, 6476 – 6481.
[14] Y. Chae, S. Mori, M. Suzuki, *Thin Solid Films* **2009**, *517*, 4260 – 4263.
[15] S. Sahoo, A. K. Arora, V. Sridharan, *J. Phys. Chem. C* **2009**, *113*, 16927 – 16933.
[16] a) T. Jirsak, J. Dvorak, J. A. Rodriguez, *Surf. Sci.* **1999**, *436*, L683 – L690; b) J. Moulder, W. Stickle, P. Sobol, K. Bomben, *Handbook of X-ray photoelectron spectroscopy*, *2nd ed.*, PerkinElmer, Minnesota, **1992**.
[17] a) L. Bonneviot, G. Haller, *J. Catal.* **1988**, *113*, 96 – 105; b) T. Berger, M. Sterrer, O. Diwald, E. Knözinger, *ChemPhysChem* **2005**, *6*, 2104 – 2112; c) M. Chiesa, M. C. Paganini, S. Livragh, E. Giamello, *Phys. Chem. Chem. Phys.* **2013**, *15*, 9435 – 9447; d) A. Brückner, *Chem. Soc. Rev.* **2010**, *39*, 4673 – 4684; e) J. M. Coronado, A. Maira, J. C. Conesa, K. Yeung, V. Augugliaro, J. Soria, *Langmuir* **2001**, *17*, 5368 – 5374.
[18] a) E. Serwicka, *Colloid Surf.* **1985**, *13*, 287 – 293; b) N. M. Dimitrijevic, Z. V. Saponjic, B. M. Rabatic, O. G. Poluektov, T. Rajh, *J. Phys. Chem. C* **2007**, *111*, 14597 – 14601.
[19] a) C. Di Valentin, G. Pacchioni, A. Selloni, S. Livraghi, E. Giamello, *J. Phys. Chem. B* **2005**, *109*, 11414 – 11419; b) G. Barolo, S. Livraghi, M. Chiesa, M. C. Paganini, E. Giamello, *J. Phys. Chem. C* **2012**, *116*, 20887 – 20894.

Received: July 22, 2015
Published online: October 2, 2015

